




# Analysis of structural, electrical, and levitation properties of (RE: Nd, Sm, Gd) BCO-358 superconducting ceramics prepared by a modified MPMG technique

Sezai Kutuk<sup>1,\*</sup>  and Suleyman Bolat<sup>2</sup>

<sup>1</sup>Department of Marine Engineering, Faculty of Turgut Kiran Maritime, Recep Tayyip Erdogan University, 53900 Rize, Turkey

<sup>2</sup>Department of Physics, Faculty of Science, Karadeniz Technical University, 61080 Trabzon, Turkey

Received: 27 May 2021

Accepted: 5 November 2021

Published online:  
3 January 2022

© The Author(s), under exclusive licence to Springer Science+Business Media, LLC, part of Springer Nature 2021

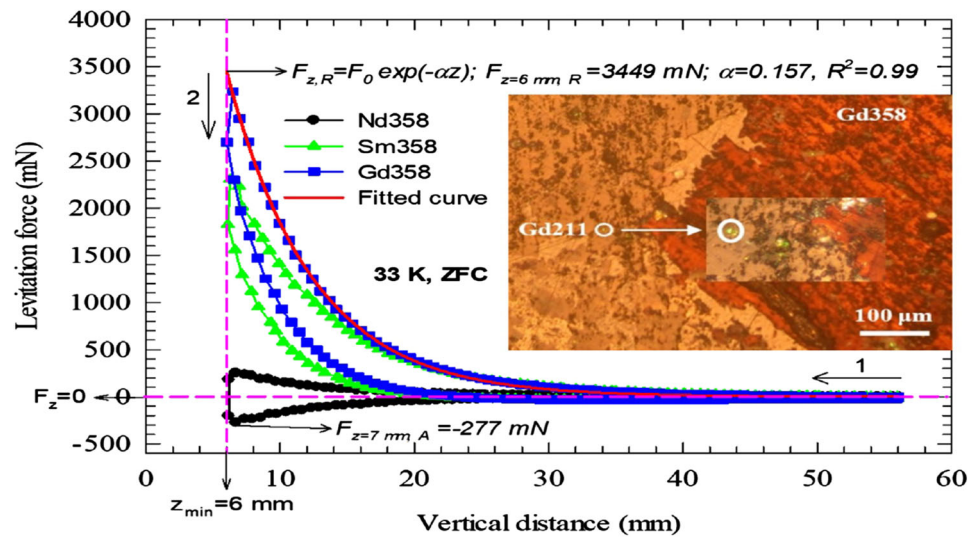
## ABSTRACT

RE<sub>3</sub>(Nd, Sm, Gd)Ba<sub>5</sub>Cu<sub>8</sub>O<sub>y</sub> (RE358) superconducting ceramics were prepared by a modified Melt-Powder-Melt-Growth (MPMG) technique. The structural properties of samples were examined with bulk density, an X-Ray Diffractometer (XRD), a Polarized Optical Microscope (POM); their electrical properties were investigated with a four-point probe method; their levitation properties were measured with a closed-cycle cryostat levitation system. In the XRD measurement, minor phases such as RE211 were detected along with the superconductor phase. In the POM micrograph, it was observed that the Gd358 MPMG sample had fewer weak-link, bigger superconductor grains, smaller RE211 particles, and lower pore. The best  $T_c^{\text{onset}}$ ,  $T_c^{\text{offset}}$ , and  $\Delta T_c$  transition temperatures under applied magnetic field were found in the Gd358 MPMG sample from the electrical resistance measurement. The lowest  $\beta$  value obtained from the activation energy was calculated as 0.23 for the Gd358 MPMG sample; that is, this value is quite well compared to the literature. It was concluded from the levitation measurement that the Gd358 MPMG sample had the maximum  $F_{z,R}$  value at all temperatures. A strong correlation was determined between temperature and  $\alpha$  value estimated from  $F_{z,R}$  equation. It is hoped that the Gd358 sample would be used in superconducting devices from the point of view of technique and economics.

Handling Editor: Joshua Tong.

Address correspondence to E-mail: sezai\_kutuk@hotmail.com; sezai.kutuk@erdogan.edu.tr

## GRAPHICAL ABSTRACT



## Introduction

(RE: Nd, Sm, Gd)BCO ceramic family has been studied intensively in science and technology since the discovery of the high-temperature superconductor (HTSC) in 1987, and thus, it is demanded in the industry as well. (RE)BCO family has a high carrying capacity of electrical current in the strong magnetic field due to large flux pinning [1]. Because the microstructure of this family includes large grain, both the levitation force ( $F_z$ ) and the trapped field ( $B_p$ ) are high [2]. Applications such as magnetic separation, a magnetic drug delivery system, a desktop MRI system, a wind turbine generator, and a motor for ship propulsion make bulk (RE)BCO superconductors desirable owing to lower volume, less weight, and lower running cost [3]. Furthermore, high  $F_z$  values of these superconductors open up an opportunity for a wide range of applications: MagLev train, frictionless magnetic bearing, hysteresis motor, generator, a flywheel energy storage system, permanent magnet, and so on [4].

The fabrication of Y-based HTSC is easier in comparison with Bi-, Tl-, and Hg-based HTSC. In addition, a distinguishable advantage of Y-based HTSC is that large domain crystals can be grown by melt-

texturing techniques providing good microstructural and electrical properties [5]. Critical (transition) temperature ( $T_c$ ) is a significant superconductivity property in terms of technology. Up to the present,  $T_c$  values determined for the YBCO family are approximately 92 K for Y123 compound/sample [6], 80 K for Y124 sample [7], 40 K for Y247 sample [8], and 102 K for Y358 sample [9]. Here, the Y358 sample which is above liquid nitrogen temperature (77 K) and has the highest  $T_c$  value draws attention in practice from the point of view of economics.

Topal et al. [10] published that the resistivity versus temperature ( $\rho-T$ ) measurements showed the  $T_c^{\text{onset}}$  as 97.5, 97, and 95 K for the Y358, Sm358, and Nd358 samples, respectively. The first two  $T_c^{\text{onset}}$  values are larger than the largest value measured for the (RE)BCO family. In addition,  $T_c^{\text{offset}}$  value is  $\sim 70$  K for Y358 sample,  $\sim 80$  K for Sm358 sample, and  $< 50$  K for Nd358 sample under  $\mu_0 H_a = 1000$  mT of the applied magnetic field. More clearly, Sm358 sample is more durable against the magnetic field.

Aliabadi et al. [11] reported that  $T_c^{\text{onset}}$  value for Gd358 sample was 97 K and this value was higher than the value of Gd123 sample. Besides,  $\beta$  value (power factor in activation energy ( $U_0$ )) under the magnetic field applied between  $H_a = 1-15$  kOe was calculated as 0.41 for the Gd358 sample and 0.60 for

the Y358 sample. In other words, the sensitivity of the Gd358 sample to the magnetic field is less than the Y358 sample.

Rekaby et al. [12] determined that the  $T_c$  values of  $Y_{3-x}Nd_xBa_{5-x}Ca_xCu_8O_{18}$  sample deteriorated by substituting from  $x = 0.0$  to  $0.4$ , but the critical current density at the zero temperature ( $J_c(0)$ ) calculated from  $U_0$  for  $\mu_0 H_a = 0.00$ – $4.44$  kG improved with the increase of  $x$ . This improvement was attributed to the lattice defects which intensify the flux pinning.

Kutuk et al. [13] declared that Y358 sample reveals a rise of 10 K for  $T_c^{\text{offset}}$  and a narrowing of 41 K for  $\Delta T_c$  (broadening of the resistance transition) at  $\mu_0 H_a = 5$  T in comparison with the Y123 sample. Furthermore, the temperature equivalent to the irreversibility field of the Y358 sample ( $\mu_0 H_{irr}(T)$ ) and also the temperature equivalent to the upper critical field ( $\mu_0 H_{c2}(T)$ ) are 41 K and 2 K higher than the Y123 sample, in turn.

Bolat and Kutuk [14] investigated that under the zero-field-cooled (ZFC) regime at 77 K, the repulsive levitation force ( $F_{z,R}$ ) of the Y358 sample was 71% more than Y123 sample and also the attractive levitation force ( $F_{z,A}$ ) was 51% higher than the Y123 sample. Similarly, under the field-cooled (FC) regime, the  $F_{z,A}$  value of the Y358 sample was 45% more than the Y123 sample and the  $F_{z,R}$  value was 64% better than the Y123 sample.

Although there have been many studies since 2009 on the structural, electrical, and levitation properties of Y358 samples, there are few studies on Nd358, Sm358, and Gd358 (RE358) samples. Therefore, the aim of this study was to analyze the levitation properties of RE358 samples in addition to the structural and electrical properties.

## Materials and methods

### Production of materials

$Nd_2O_3$  (99.9%, Aldrich),  $Sm_2O_3$  (99.99%, Sigma-Aldrich),  $Gd_2O_3$  (99.99%, Alfa-Aesar),  $BaCO_3$  (99.999%, Aldrich) and  $CuO$  (99.99%, Aldrich) powders with high purity weighed in an atomic ratio of 3:5:8 on an electronic balance of 0.1 mg precision. These powders were first mixed by hand in agate and then by a high-energy planetary ball mill (Retsch, PM100). The milling process was carried out simply using a 250 ml zirconia vial, three zirconia balls of

20 mm size and 25 g mass, a rotation speed of 400 rpm, a milling time of 30 min, a break of 3 min after every 15 min, and a ball-to-powder weight ratio (BPR) of  $\sim 2:1$ . The mixed powders were placed in an alumina crucible and calcined in a chamber furnace (Lenton, Eurotherm 818 Controller / Programmer) for 12 h at 840 °C. The powders were thoroughly mixed again in the mill for homogeneity and then calcined a second time.

Quenching procedure was performed on the calcined powders as given in another study [15]. The quenched powder/the molten material was pulverized by grinding in the ball mill to obtain both a smaller-sized powder and a more homogeneous powder (Melt-Powder stage). The milling process was fulfilled simply by a 250 ml zirconia vial, three zirconia balls of 20 mm size and 25 g mass, a rotation speed of 400 rpm, a milling time of 90 min, a break of 3 min after every 15 min, and a BPR of  $\sim 3:1$ . Then milled powder was pressed into 4 g under a pressure of 300 MPa using a 13 mm cylinder geometry mold [13].

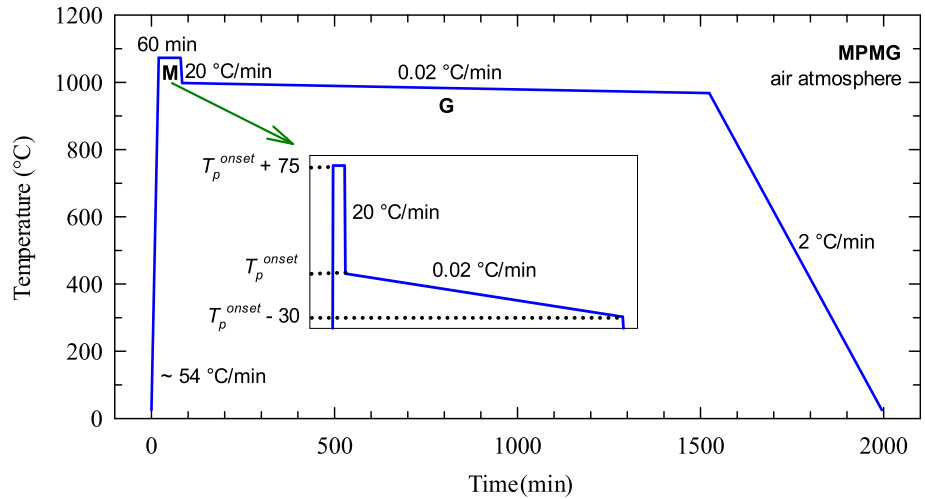
Pellet samples were sintered for the Melt-Growth stage in air atmosphere in a tube furnace (Lenton, Eurotherm 818 Controller/Programmer) as seen in Figure 1 after onset values of peritectic temperature ( $T_p^{\text{onset}}$ ) were determined from the Differential Thermal Analysis (DTA) measurement in order to obtain a better crystal.

All sintered samples were annealed simultaneously in the oxygen atmosphere as represented in another study [13]. Finally, bulk  $RE_3(Nd, Sm, Gd)Ba_5Cu_8O_y$  ceramic samples were produced using the modified Melt-Powder-Melt-Growth (MPMG) technique. This technique was preferred in the melting techniques for the purpose of identification the typical characteristics of RE358 samples, which are not well known, because of fact that the production cost is low and production time is short.

### Measurements

The thermal phase transitions of the quenched powders before the sintering process were deduced from a DTA device (SII (Seiko Inst. Inc.), Exstar 6300). The 20 mg powder was placed in the device in a platinum crucible. The mass precision was 0.01  $\mu\text{g}$  and the reference powder was  $Al_2O_3$ . Measurements were taken in dry air at a speed of 10 °C/min and a temperature range from 20 to 1300 °C.

**Figure 1** Schematic diagram of the sintering process. M, G, and  $T_p^{onset}$  indicate Melt, Growth, and onset of peritectic temperature, in turn.



The bulk densities ( $\rho_s$ ) of all samples/HTSCs were obtained from a densitometer based on Archimedes' principle. The test apparatus consists of a low viscosity diethyl phthalate ( $C_{12}H_{14}O_4$ ) liquid with a density ( $\rho_l$ ) of 1.122 g/cm<sup>3</sup> at 20 °C and a digitally controlled microbalance (Sartorius, BP 110 S) with a precision of 0.1 mg. The cylindrical samples in the original volume of about  $\pi 6^2 \times 6$  mm<sup>3</sup> were first weighed in the air environment ( $m_a$ ) and then weighed in the liquid environment ( $m_l$ ) at 30 s after being thrown into the liquid. The density of the sample was estimated from Eq. (1).

$$\rho_s = \rho_l m_a / (m_a - m_l) \tag{1}$$

Phase compositions (main phase, secondary phases) and crystal structures ((hkl) planes, lattice parameters) of the samples were analyzed by a powder X-Ray Diffractometer (XRD; Rikagu, D/Max III). The samples in the original volume were placed vertically in the diffractometer and the operating conditions were adjusted to a voltage of 40 kV, a current of 30 mA, scanning range of  $20^\circ \leq 2\theta \leq 80^\circ$ , a step width of  $0.05^\circ$ , and a speed of  $3^\circ/\text{min}$ . In addition, measurements were fulfilled from the top surface of the samples under air atmosphere at room temperature using  $CuK_\alpha$  X-ray with a wavelength of 1.5418 Å.

The morphological properties of the samples in the original volume such as grain size, distribution, and orientation, grain boundary, secondary phases, pore, and macro-crack were observed via Polarized Optical Microscope (POM; Nikon, ECLIPSE ME600). After the sanding process was performed to correct the smoothness on the top surface of the samples,

polishing was carried out with diamond powders of 23, 10 and 1 μm, respectively. After this process, micrographs were taken from the top surface of the sample at magnifications of  $\times 320$  and  $\times 640$ .

The low-temperature DC electrical properties of the samples under the external magnetic field such as  $T_c$ ,  $\Delta T_c$ ,  $U_0$ ,  $\mu_0 H_{irr}$ ,  $\mu_0 H_{c2}$  values were examined by a computer-controlled closed-cycle cryostat system. This system contains a liquid helium superconducting coil magnet device (CRYO Industries of America), a programmable current source (Keithley, model 220), and a nano voltmeter (Keithley, model 2182A). The samples were cut into a rectangular prism, approximately  $3 \times 8 \times 2$  mm<sup>3</sup> for measurement in the cryostat. The measurement was carried out with a four-point probe method and here, a silver paste was used in order to minimize the resistance. Furthermore, the data were transferred into a computer environment at a temperature range from 5 to 150 K under the ZFC regime, a stable DC of 5 mA, and a stable DC magnetic field of 0; 0.25; 0.50; 1; 5 T.

The levitation properties of the samples in the original volume were investigated by a computer-controlled device consisting of a combination of closed-cycle cryostat and levitation force systems. Detailed information is available in another study [16]. After the samples were cooled to 33 K, 50 K, and 77 K, their levitation forces were measured in the ZFC regime.

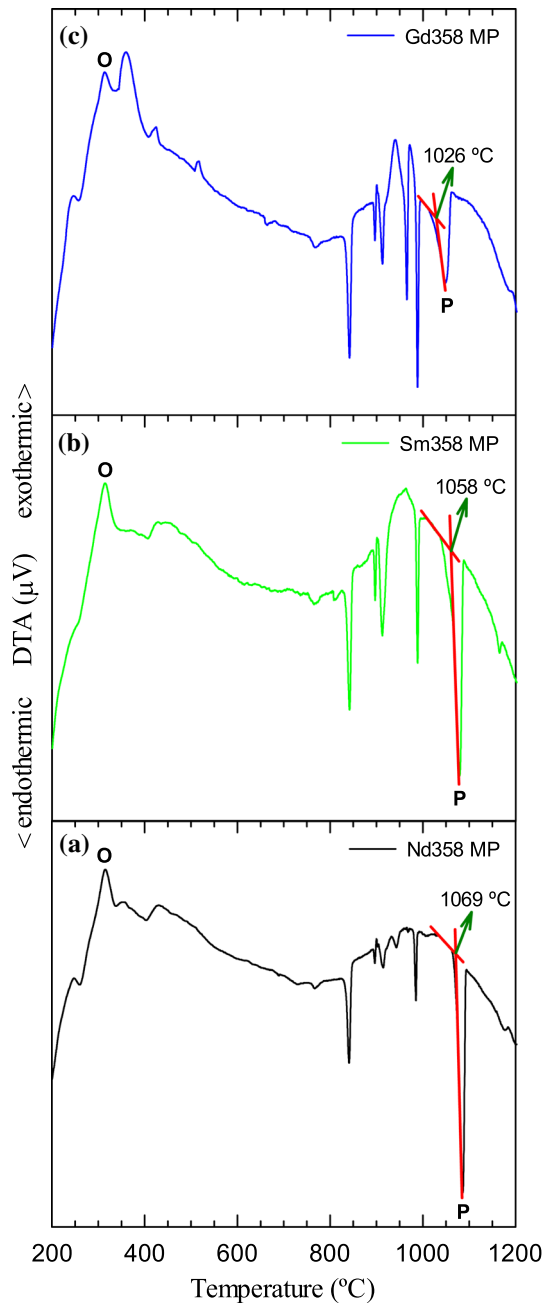


**Figure 2** DTA curves of **a** Nd358 MP, **b** Sm358 MP, and **c** Gd358 MP quenched powders. MP, O, and P denote Melt-Powder, Oxygen, and Peritectic, respectively.

## Results and discussion

### Thermal analysis

Figure 2a, b, and c, respectively, show the DTA curves of Nd358 MP (Melt-Powder), Sm358 MP, and Gd358 MP quenched powders. Exothermic peaks in the range of 200 °C to 550 °C indicate the oxygen

absorption temperature. Also, endothermic peaks in the range of 650 °C to 1200 °C refer to decomposition and/or formation temperatures. From these results, the melting temperature and crystal growth temperature values in the sintering process, as well as the temperature values in the oxygenation process were determined. The  $T_p^{\text{onset}}$  values of DTA curves were found out as 1069 °C for Nd358 MP, 1058 °C for Sm358 MP, and 1026 °C for Gd358 MP. These values coincided well with  $T_p$  values of 1090 °C for Nd, 1060 °C for Sm, and 1030 °C for Gd in another study [17].

In the sintering process, the constant temperature of  $T_p^{\text{onset}} + 75$  °C ( $\text{RE}_2\text{BaCuO}_5$  (RE211) solid phase + Liquid phase, based on the phase diagram reported in the first MPMG technique [18]) for melting and the temperature range from  $T_p^{\text{onset}}$  to  $T_p^{\text{onset}} - 30$  °C (RE358 solid phase + Liquid phase) for crystal growth were chosen for systematicity. In addition, a similar sintering process was previously carried out at 1130 °C for melting and 990 °C for crystal growth to produce the modified Y358 MPMG sample, which has large superconducting grains and high levitation force [14].

### Structural analysis

Figure 3 demonstrates the bulk density and porosity of all samples. Bulk densities for Nd358, Sm358, and Gd358 MPMG samples were measured as 6.06, 6.16, and 6.44  $\text{g}\cdot\text{cm}^{-3}$ , in turn. Since the theoretical densities of Nd123, Sm123, and Gd123 compounds are,

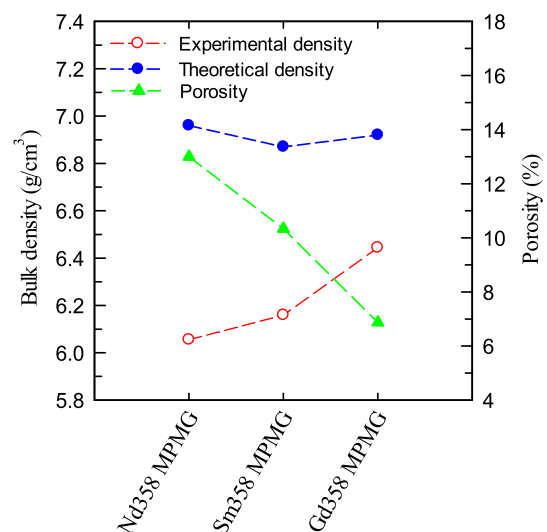


**Figure 3** Bulk densities (left side) and porosities (right side) of all samples.

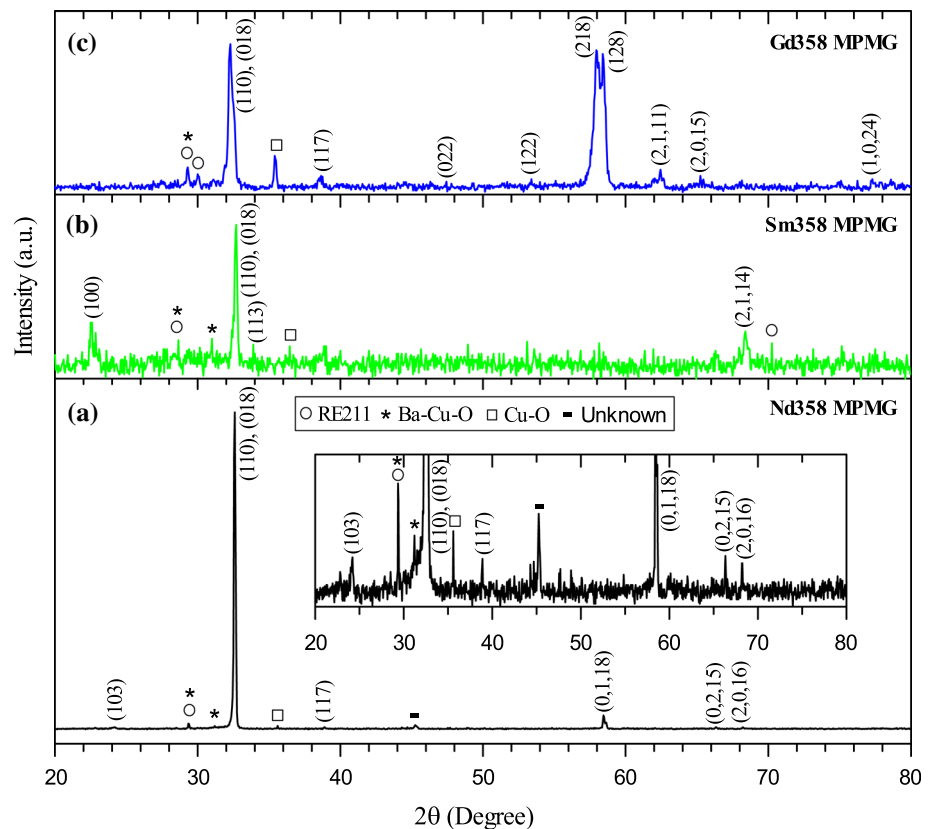


respectively, 6.96 [19], 6.87 [20], and 6.92 [21]  $\text{g}\cdot\text{cm}^{-3}$ , the porosity values were calculated as 13.00%, 10.34%, and 6.87% (right side of Figure 3). These results comply with the porous structure of bulk superconductor and denote that the sample with the minimum amount of pore in the structure is Gd358 MPMG.

The XRD patterns of all samples are shown in Figure 4. It was determined that the main phase indicated by Miller indices/(hkl) planes was the superconducting phase. The peaks of the highest intensity for the samples are (110) and (018), and also these peaks accord with the literature [9, 22]. The twin peaks (218) and (128) observed in the Gd358 MPMG sample at  $58^\circ$  are in agreement with the peaks determined by Aliabadi et al. [9]. The crystal structure of the Gd358 MPMG sample is orthorhombic because this is similar to twin peaks (123) and (213) of the RE123 orthorhombic structure observed at  $58^\circ$  [23]. Furthermore, the RE211, Ba–Cu–O, Cu–O impurity phases, and unknown phase demonstrated with different symbols were identified. Although the impurity phases appeared in all samples, their ratios were found to be different. In other words, the Ba–

Cu–O phase was mostly in the Nd358 and Sm MPMG samples (Figure 4a, b), whereas the RE211 phase was mainly in the Gd358 MPMG sample (Figure 4c). However, since the impurity phases are not dominant compared to the superconducting phase, it can be understood that the superconducting forming ratio is quite large [24]. The XRD patterns obtained by Rekaby et al. [12], Ghahramani et al. [25], and Shoushtari et al. [26] are similar to the XRD patterns in Figure 4. Rekaby et al. [12] calculated the relative volume fraction percentages of the Y358 superconducting phase as high (from 92 to 84%) and the relative volume fraction percentages of the other phases as low (from 8 to 16%). As a result, they found that as the percentages of the other phases increased, the  $T_c^{\text{offset}}$  value decreased, whereas both  $U_0$  and calculated  $J_c(0)$  values improved. Ghahramani et al. [25] determined that with a small increase in the intensity of the minor Y211 phase, the  $T_c^{\text{offset}}$  value was reduced, while the differentiation of resistivity value increased. Shoushtari et al. [26] made Ag additives (1 and 2 wt.%) with different particle sizes (30, 700, and 1000 nm) to the Y358 sample with minor secondary phases, and they estimated that the relative volume

**Figure 4** XRD patterns for a Nd358, b Sm358, and c Gd358 MPMG samples. (hkl) and symbols represent, respectively, superconducting and non-superconducting phases. The inset figure is for low intensity.



fraction percentage of the Y358 phase in the superconducting phases (from 62% to 78%) increased with the 700 nm Ag additives. Thus, they decided that the pores in the microstructure diminished and also both  $T_c^{\text{offset}}$  and transport  $J_c(0)$  values enhanced.

The (hkl) value and the interplanar spacing obtained from the diffraction pattern were estimated using a computer program including the least square method, and besides the lattice parameters, volumes and orthorhombicities of the samples were calculated as listed in Table 1. All samples have orthorhombic lattice system. The  $c$ -parameter gradually decreased for Nd358, Sm358, and Gd358 MPMG samples, in turn. This can be attributed to the ionic radii of the samples  $r_{\text{Nd}^{+3}} = 1.109 \text{ \AA}$ ,  $r_{\text{Sm}^{+3}} = 1.079 \text{ \AA}$ ,  $r_{\text{Gd}^{+3}} = 1.053 \text{ \AA}$  (coordination number: 8) [17]. Orthorhombicity was estimated from the  $\Delta = |a - b| / (a + b) \times 100$  formula. The orthorhombicity is the best in the Gd358 MPMG sample with 1.20% and the worst in the Nd358 MPMG sample with 0.56%. From this data, it was concluded that the Nd358 MPMG sample was closer to the tetragonal structure and its value of 0.56% was less than the value of 0.85% estimated by Aliabadi et al. [9].

A relationship between the  $c$ -parameter and the oxygen content ( $y$ ) [27] was developed as the formula  $y/3 = 75.250 - 5.856c/2.663$  for RE358 samples. The coefficient of 2.663 here is the ratio of  $c$ -parameters calculated by Bolat and Kutuk [14] from the XRD pattern for Y358 and Y123 MPMG samples; that is, it is  $31.089 \text{ \AA} / 11.675 \text{ \AA}$ . As can be seen from Table 1, the  $y/3$  values of Nd358, Sm358, and Gd358 MPMG samples are accordant with the literature [28]. The  $y/3$  of the Gd358 MPMG sample is 6.74 higher than the others. It is well known that the crystal structure is orthorhombic if  $y/3$  is equivalent to 6.5–7.0, and also the orthorhombicity increases as the  $y/3$  value approaches to 7.0, thus increasing the  $T_c^{\text{offset}}$  value [27].

Figure 5a, b, and c, respectively, display the POM micrographs of Nd358, Sm358, and Gd358 MPMG samples. Superconducting grains (crystals) were generally larger than  $100 \mu\text{m}$  in all samples.

Nevertheless, the Sm358 MPMG sample (Figure 5b) demonstrated locally large grains and small grains. While weak-link between the grains was the most in the Nd358 MPMG sample (Figure 5a), large grains were the highest in the Gd358 MPMG sample (Figure 5c). In light of this data, it is realized that the superconductivity of Gd358 MPMG sample is good [29]. Additionally, the presence of superconducting grains in different colors arises from the different crystal orientations [24]; that is, the sample is polycrystalline.

In the structure, non-superconducting (secondary) green phase (RE211), barium-rich phase (Ba-r), pore (P), and macro-crack (MAC) were observed. Gd358 MPMG sample has the most RE211 phase. The Gd211 phase is homogeneously distributed throughout the sample, with a size of less than  $5 \mu\text{m}$ , particularly agglomerated in grain boundaries and pores (the inset of Figure 5c). It is clear that such RE211 phase/particles increase not only the  $J_c$  value [30] but also the  $F_z$  value [31].

The Nd358 MPMG sample has the most Ba-r phase, P, and the weak-link, whereas the Gd358 MPMG sample has the least. The Ba-r phase observed in the Nd358 MPMG sample and the Gd211 phase observed in the Gd358 MPMG sample confirm XRD measurements. If the weak-link, P, and MAC are low, bulk density becomes high. Therefore, this result complies with bulk density and porosity results. According to a previous study [32], these findings point out that the  $J_c$  and  $T_c$  values of the Gd358 MPMG sample would be high.

## Electrical analysis

Electrical resistance measurements ( $R$ - $T$ ) of the samples under the applied magnetic field ( $\mu_0 H_a$ ) are given in Figure 6 and also their  $T_c$  values are given in Table 2.

When the samples were examined, the highest  $T_c^{\text{onset}} = 97.98 \text{ K}$ , the largest  $T_c^{\text{offset}} = 90.44 \text{ K}$ , and the narrowest  $\Delta T_c$  ( $T_c^{\text{onset}} - T_c^{\text{offset}}$ ) =  $7.54 \text{ K}$  in the absence of magnetic field (0 T) were in the Gd358

**Table 1** Lattice parameters of the samples

| Sample     | $a$ (Å) | $b$ (Å) | $c$ (Å) | $V$ (Å <sup>3</sup> ) | Orthorhombicity (%) | Oxygen content |
|------------|---------|---------|---------|-----------------------|---------------------|----------------|
| Nd358 MPMG | 3.8683  | 3.8250  | 31.1917 | 461.52                | 0.56                | 6.66           |
| Sm358 MPMG | 3.9208  | 3.8512  | 31.1665 | 470.61                | 0.90                | 6.71           |
| Gd358 MPMG | 3.9263  | 3.8334  | 31.1548 | 468.91                | 1.20                | 6.74           |

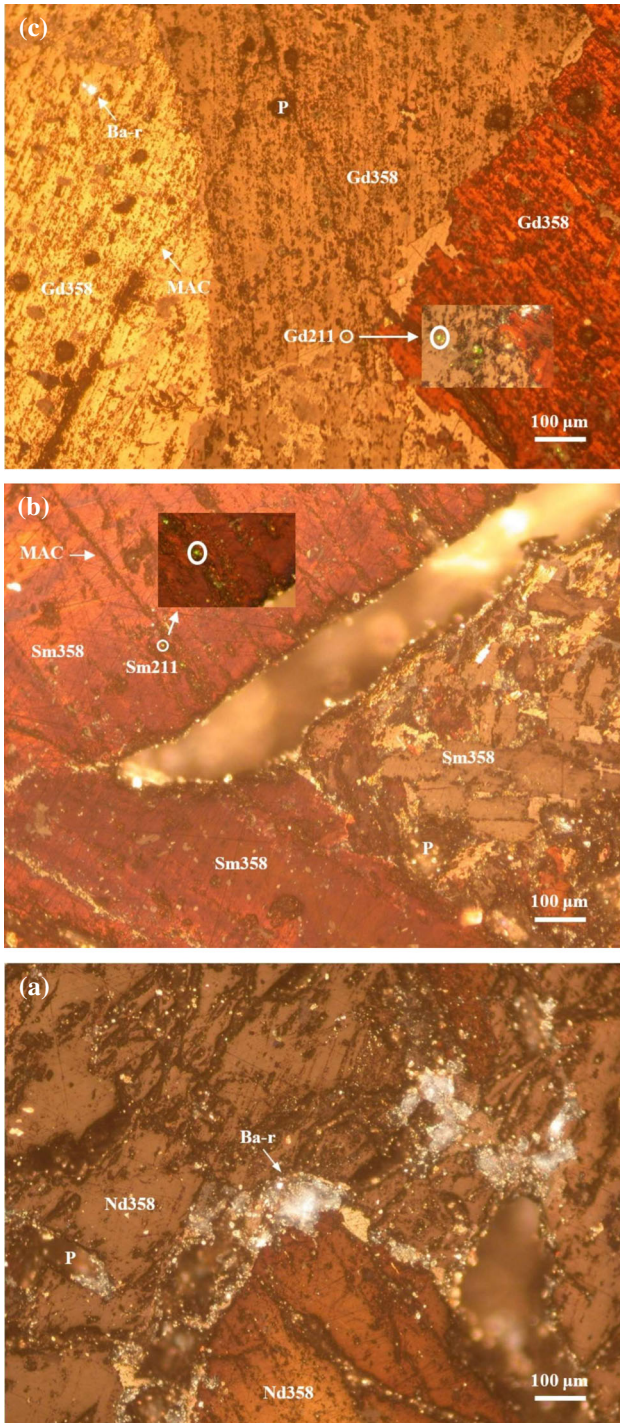


**Figure 5** POM micrographs under  $\times 320$  magnification for **a** Nd358, **b** Sm358, and **c** Gd358 MPMG samples. The inset figures are  $\times 640$  magnification. RE211, Ba-r, P, and MAC express green phase, barium-rich phase, pore, and macro-crack, in turn.

MPMG sample. On the other hand, the highest  $T_c^{\text{onset}} = 97.19$  K, the largest  $T_c^{\text{offset}} = 86.34$  K, and

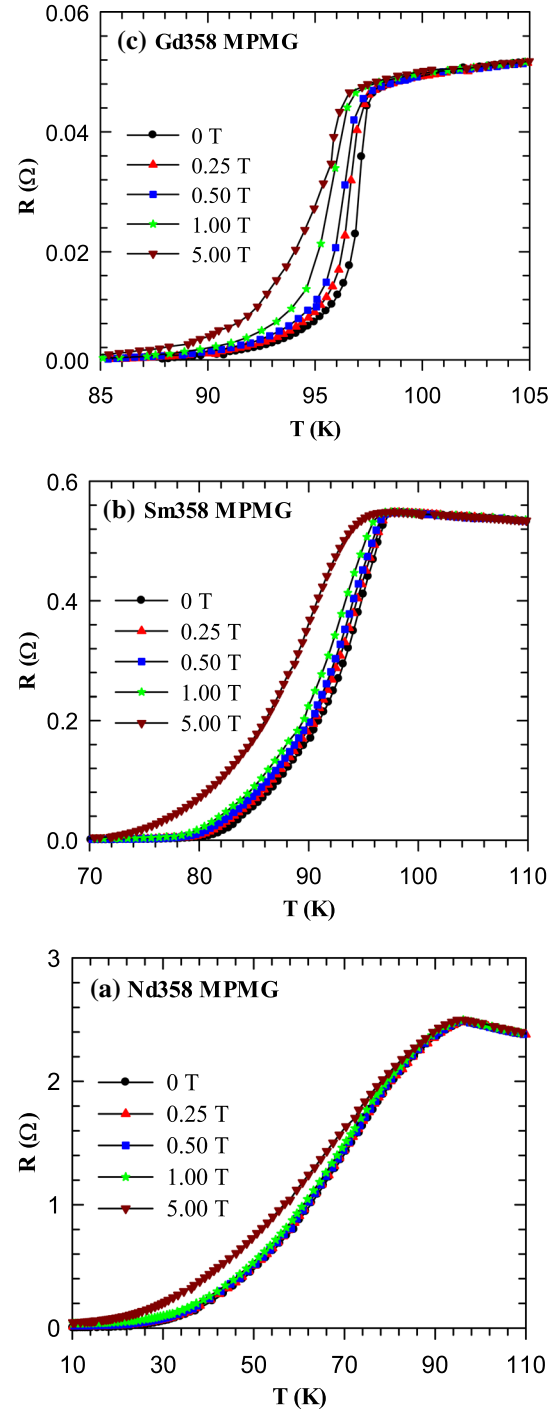


**Figure 6** Temperature dependence of resistance at different magnetic fields for **a** Nd358, **b** Sm358, and **c** Gd358 MPMG samples.

the narrowest  $\Delta T_c = 10.85$  K in the presence of the maximum magnetic field (5 T) were again in the Gd358 MPMG sample. In contrast, the lowest  $T_c^{\text{onset}} = 96.16$  K, the smallest  $T_c^{\text{offset}} = 29.05$  K, and the widest  $\Delta T_c = 67.11$  K at 0 T were in the sample



**Table 2** Critical temperatures of the samples under varying magnetic fields

| Sample     | Temperature (K)            | Applied magnetic field ( $\mu_0 H_a$ ) |        |       |       |       |
|------------|----------------------------|--|--------|-------|-------|-------|
|            |                            | 0 T                                    | 0.25 T | 0.5 T | 1 T   | 5 T   |
| Nd358 MPMG | $T_c^{\text{onset}}$       | 96.16                                  | 95.90  | 95.86 | 95.71 | 95.55 |
|            | $T_c^{\text{mid}}$ (50% R) | 66.94                                  | 66.52  | 66.16 | 65.65 | 62.21 |
|            | $T_c^{\text{offset}}$      | 29.05                                  | 27.01  | 25.72 | 23.02 | 15.11 |
|            | $\Delta T_c^{\text{mid}}$  | 29.22                                  | 29.38  | 29.70 | 30.06 | 33.34 |
|            | $\Delta T_c$               | 67.11                                  | 68.89  | 70.14 | 72.69 | 80.44 |
| Sm358 MPMG | $T_c^{\text{onset}}$       | 97.51                                  | 97.30  | 96.98 | 96.70 | 96.26 |
|            | $T_c^{\text{mid}}$ (50% R) | 92.79                                  | 92.20  | 91.85 | 91.09 | 88.01 |
|            | $T_c^{\text{offset}}$      | 80.89                                  | 79.79  | 79.24 | 78.40 | 72.42 |
|            | $\Delta T_c^{\text{mid}}$  | 4.72                                   | 5.10   | 5.13  | 5.61  | 8.25  |
|            | $\Delta T_c$               | 16.62                                  | 17.51  | 17.74 | 18.30 | 23.84 |
| Gd358 MPMG | $T_c^{\text{onset}}$       | 97.98                                  | 97.79  | 97.66 | 97.43 | 97.19 |
|            | $T_c^{\text{mid}}$ (50% R) | 96.90                                  | 96.42  | 96.07 | 95.39 | 94.53 |
|            | $T_c^{\text{offset}}$      | 90.44                                  | 90.02  | 89.71 | 88.91 | 86.34 |
|            | $\Delta T_c^{\text{mid}}$  | 1.08                                   | 1.37   | 1.59  | 2.04  | 2.66  |
|            | $\Delta T_c$               | 7.54                                   | 7.77   | 7.95  | 8.52  | 10.85 |

Nd358 MPMG. On the other hand, the lowest  $T_c^{\text{onset}} = 95.55$  K, the smallest  $T_c^{\text{offset}} = 15.11$  K, and the widest  $\Delta T_c = 80.44$  K at 5 T were again in the Nd358 MPMG sample. Based on these findings, the best quality sample was Gd358 MPMG, while the worst sample was Nd358 MPMG. The results obtained from the electrical measurements and the structural properties comply with very well each other. Therefore, it can be inferred that the use of Gd358 MPMG superconducting material is remarkable in engineering applications.

The poor  $T_c$  values of the Nd358 MPMG sample were due to the fact that the production technique of all samples was chosen the same for comparison. However, if a reduced oxygen atmosphere was used in the sintering process, the Nd and Ba elements would be present in the sites where they should be, so that it would be possible to obtain high  $T_c^{\text{offset}}$  [33]. Topal et al. [10] declared that the transport temperatures of the Nd358 sample prepared by the solid-state reaction (SSR) technique are  $T_c^{\text{onset}} = 95$  K and  $T_c^{\text{offset}} < 50$  K at 1 T. Besides, Rekaby et al. [12] reported that the  $T_c$  (the maximum of  $d\rho(T)/dT$ ) of the  $Y_{3-x}Nd_xBa_{5-x}Ca_xCu_8O_{18}$  sample prepared by the SSR technique decreased to 85 K for  $x = 0.4$ . Thus, the literature results agree with the results of this study.

The two-step state, where the first step was attributed to the intra-grain region and the second step was ascribed to the inter-grain region [34], observed in the transition from the normal state to the superconducting state when the field was applied

was not ascertained in these samples. This is because the MPMG technique is more resistant to the magnetic field than the conventional SSR technique [13, 15]. Since larger textured RE123 grains, smaller size and homogeneously distributed RE211 particles, and fewer weak-links can be attained thanks to the peritectic reaction described as the  $RE211 + \text{Liquid} \rightarrow RE123$  of the MPMG technique, the flux pinning force ( $F_p$ ) get stronger [18]. Furthermore, these interpretations also explain that the Gd358 MPMG sample has better  $T_c$  values than the other two samples. Aliabadi et al. stated that the  $T_c^{\text{onset}}$  is 97 K and  $\Delta T_c$  is 3 K for a Gd358 compound, and these values are better than those of the Gd123 compound. Their findings support the findings of this study. The  $T_c^{\text{offset}}$  value found by Aliabadi et al. [11] was approximately 77 K at 2 kOe and about 73 K at 15 kOe, whereas the  $T_c^{\text{offset}}$  value measured in this study was approximately 90 K at 0.25 T ( $\approx 2.5$  kOe) and about 86 K at 5 T. In other words, it was concluded that the  $T_c^{\text{offset}}$  value of this study was less sensitive to the magnetic field owing to the production process.

The increment difference between  $\Delta T_c$  and  $\Delta T_c^{\text{mid}}$  with increasing magnetic field means that the inter-granular region (Josephson junctions) is affected more by the field. Likewise, it was determined that  $T_c^{\text{onset}}$  value diminished slightly but  $T_c^{\text{offset}}$  value decreased significantly by increasing the field. In this way,  $\Delta T_c$  was found to be expanding. This situation is clarified by the Thermally-Activated Flux-Creep (TAFC) model [11, 35].

The temperatures corresponding to the  $\mu_0 H_{irr}$  and  $\mu_0 H_{c2}$  fields were calculated by the  $R$ - $T$  graph under  $\mu_0 H_a$  taking into account Eqs. (2 and 3) [36–38].

$$R(\mu_0 H_{irr}) = 0.1R_n; \text{ for the } \mu_0 H_{irr}(T) \tag{2}$$

$$R(\mu_0 H_{c2}) = 0.9R_n; \text{ for the } \mu_0 H_{c2}(T) \tag{3}$$

Here,  $\mu_0$  represents the permeability of free space and  $R_n$  represents the normal state resistance.

The temperatures corresponding to the irreversible and upper critical fields of all samples are listed in Table 3. When  $H_{irr}$  values are compared, the Gd358 MPMG sample has the highest temperatures which are 93.20 K at 0 T and 89.33 K at 5 T; on the other hand, the Nd358 MPMG sample has the lowest temperatures which are 41.92 K at 0 T and 32.14 K at 5 T. These findings imply that pinning ability in the inter-grain region of Gd358 MPMG sample is superior to the others [38]. In addition, the  $H_{irr}$  value at 5 T calculated for the Gd358 MPMG sample is 8.92 K better than the  $H_{irr}$  value calculated by Kutuk et al. [13] for the Y358 SSR sample. This remarkable improvement stems from probably two cases. The first case is the formation of larger superconducting grains and smaller RE211 particles in samples produced by Melt-Growth techniques [15, 29]. The second case is bigger  $B_p$  depending on stronger  $F_p$  in the GdBCO sample [3, 39].

When the  $H_{c2}$  values are analyzed, the maximum and minimum temperatures at 0 T are Gd358 MPMG sample with 97.44 K and Nd358 MPMG sample with 85.58 K, respectively. Similarly, the maximum and minimum temperatures at 5 T are Gd358 MPMG sample with 96.40 K and Nd358 MPMG sample with 83.94 K, in turn. In light of these findings, it was concluded that the Nd358 MPMG sample not only had poor pinning ability but also poor superconductivity in the intra-grain region. Furthermore, the  $H_{c2}$  value at 5 T calculated for the Gd358 MPMG

sample is 2.05 K higher than the  $H_{c2}$  value calculated by Kutuk et al. [13] for the Y358 SSR sample.

Flux pinning activation energy ( $U_0$ ) was estimated from the  $R$ - $T$  graph. Resistance data were normalized to 0 T, 100 K ( $\rho_0$ ), and its natural logarithm was calculated ( $\ln(\rho/\rho_0)$ ). Using the graph of  $\ln(\rho/\rho_0)$  versus the reverse of temperature ( $T^{-1}$ ), the  $U_0$  value was estimated from Eq. (4), the Arrhenius law [35, 40].

$$\rho(T, H) = \rho_0 \exp(-U_0(H_a)/k_B T) \tag{4}$$

Here,  $U_0(H_a)$  is the activation energy required for TAFC and  $k_B$  is the Boltzmann constant.

Arrhenius plots of the samples under different magnetic fields are shown in Figure 7. The descending linear part for the low resistivity region on this plot represents TAFC. As  $H_a$  increased for all samples, the slope of these linear plots decreased. Besides, the sample with the highest slope was Sm358 MPMG (Figure 7b), whereas the sample with the least slope was Nd358 MPMG (Figure 7a).

The variation of the activation energy of the samples to the magnetic field is depicted in Figure 8 and their values are tabulated in Table 4. Firstly, it was determined that activation energy diminished exponentially with increasing magnetic field (Figure 8a), namely it diminished linearly for the log-log graph (Figure 8b). Secondly, the activation energy of the Nd358 MPMG sample was found to be smaller than the others. The possible reason for this is that the TAFC of the Nd358 MPMG sample was easier and therefore the  $F_p$  value was lower [35]. It is obvious that excess porosity, misorientation of the grains, and weak-links reduce flux pinning energy [41]. Moreover, results of bulk density, XRD, and POM in this study support these evaluations.

After the fitted curve was drawn according to the experimental data (Figure 8b), the minimum value of  $\beta$  was obtained as 0.23 for the Gd358 MPMG sample (Table 4). Consequentially, the  $\beta$  value in this study

**Table 3** Temperature values corresponding to irreversibility and upper magnetic fields of the samples

|                       | Sample     | $\mu_0 H_a$ |        |       |       |       |
|-----------------------|------------|-------------|--------|-------|-------|-------|
|                       |            | 0 T         | 0.25 T | 0.5 T | 1 T   | 5 T   |
| $T(K), \mu_0 H_{irr}$ | Nd358 MPMG | 41.92       | 41.09  | 40.47 | 39.52 | 32.14 |
|                       | Sm358 MPMG | 84.87       | 84.12  | 83.72 | 82.92 | 78.76 |
|                       | Gd358 MPMG | 93.20       | 92.61  | 92.13 | 91.29 | 89.33 |
| $T(K), \mu_0 H_{c2}$  | Nd358 MPMG | 85.58       | 85.33  | 84.96 | 84.53 | 83.94 |
|                       | Sm358 MPMG | 96.25       | 95.92  | 95.66 | 94.99 | 92.94 |
|                       | Gd358 MPMG | 97.44       | 97.28  | 97.11 | 96.64 | 96.40 |

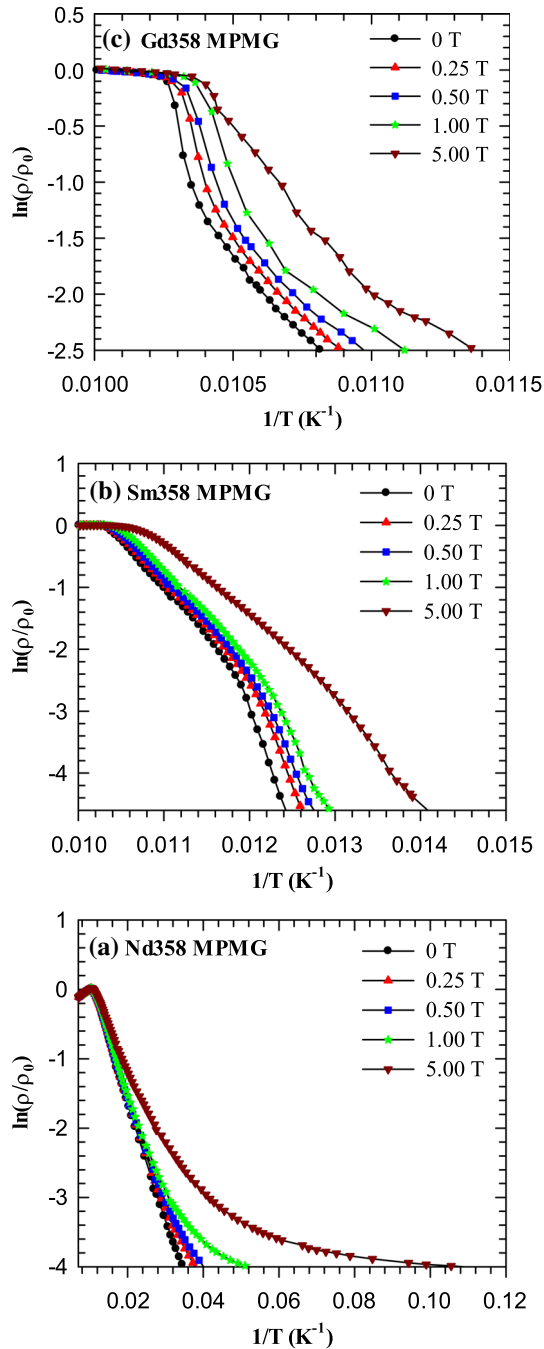


**Figure 7** The Arrhenius plots of the normalized resistivity at different magnetic fields for **a** Nd358, **b** Sm358, and **c** Gd358 MPMG samples. The activation energy was estimated from the slopes of the linear parts of the low resistivity region.

was better than 0.60 for a Gd123 SSR sample and 0.41 for a Gd358 SSR sample in a previous study [11]. Considering the power-law relation  $U_0 \propto H^{-\beta}$ , the small  $\beta$  value means that the pinning energy is higher, or a sample has less sensitivity to the

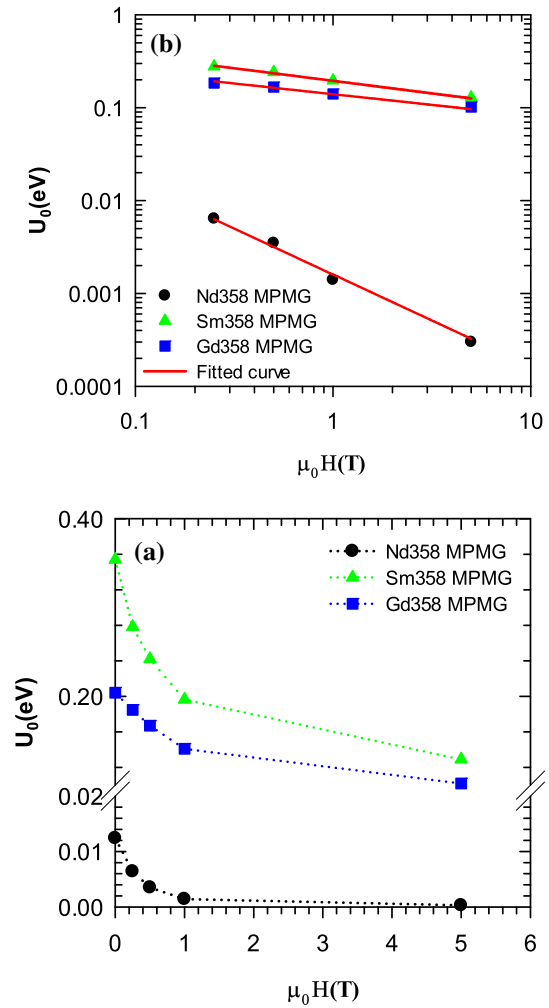


**Figure 8** Changes of activation energy with the applied field of the samples: **a** linear graph and **b** logarithmic graph.

magnetic field. The reason for the low  $\beta$  value in this study is most likely due to the production process.

### Levitation analysis

The shape of the calibrated Nd-Fe-B permanent magnet (PM) used in the apparatus and the axial magnetic field ( $B_z$ ) as a function of the vertical distance ( $z$ ) are illustrated in Figure 9. For this study, the minimum distance ( $z_{\min}$ ) between the bottom surface of the HTSC and the top surface of the PM was 6 mm, and the corresponding magnetic field ( $B_{z=6 \text{ mm}}$ ) was 3392 G.

In order to make a better comparison between the measurements, the mathematical relationship between  $F_z$  and  $z$  should be scrutinized. In this context, it is possible to divide  $F_z$  into two parts,  $F_{z,R}$  and

**Table 4** Activation energy and  $\beta$  values of the samples under varying magnetic fields

| Sample     | $U_0$ (eV), $\mu_0 H_a$ |        |        |        |        | $\beta$ |
|------------|-------------------------|--------|--------|--------|--------|---------|
|            | 0 T                     | 0.25 T | 0.5 T  | 1 T    | 5 T    |         |
| Nd358 MPMG | 0.0124                  | 0.0064 | 0.0035 | 0.0014 | 0.0003 | 0.99    |
| Sm358 MPMG | 0.3540                  | 0.2783 | 0.2420 | 0.1965 | 0.1291 | 0.27    |
| Gd358 MPMG | 0.2042                  | 0.1848 | 0.1670 | 0.1410 | 0.1020 | 0.23    |

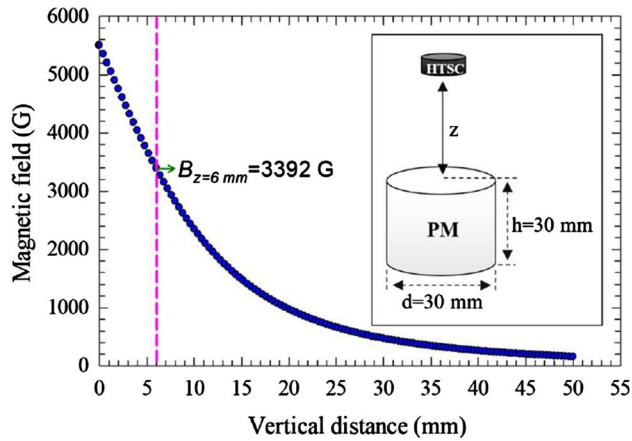


**Figure 9** The curve of a calibrated Nd–Fe–B magnet having an axial magnetic field.

$F_{z,A}$ . In the levitation force, the empirical equation of  $F_{z,R}$  (Eq. 5) was used to find the exact value of the maximum [42], and the force at  $z_{\min} = 6$  mm was calculated by a program.

$$F_{z,R} = F_0 \exp(-\alpha z) \tag{5}$$

Here,  $F_0$  symbolizes the force at  $z = 0$  mm and  $\alpha$  is a constant representing the measure of the interaction between HTSC and PM.

To analyze the levitation force measurement, Eq. (6) is important:

$$F_z = MV(dB/dz); \quad M = rJ_c A \tag{6}$$

Here,  $M$  is the magnetization,  $V$  is the volume of HTSC,  $dB/dz$  is the gradient of PM,  $r$  is the radius of the shielding current loop formed in the HTSC, and  $A$  is a constant dependent on the geometry of the HTSC [18, 43].

Figure 10a shows the variation of the levitation force against the vertical distance at 33 K of all samples. Among the samples, the largest  $F_{z,R}$  value belongs to Gd358 MPMG with 3449 mN, while the smallest  $F_{z,R}$  value belongs to Nd358 MPMG with 274 mN (Table 5). The high  $F_{z,R}$  value can be attributed to the large superconducting grains of the Gd358

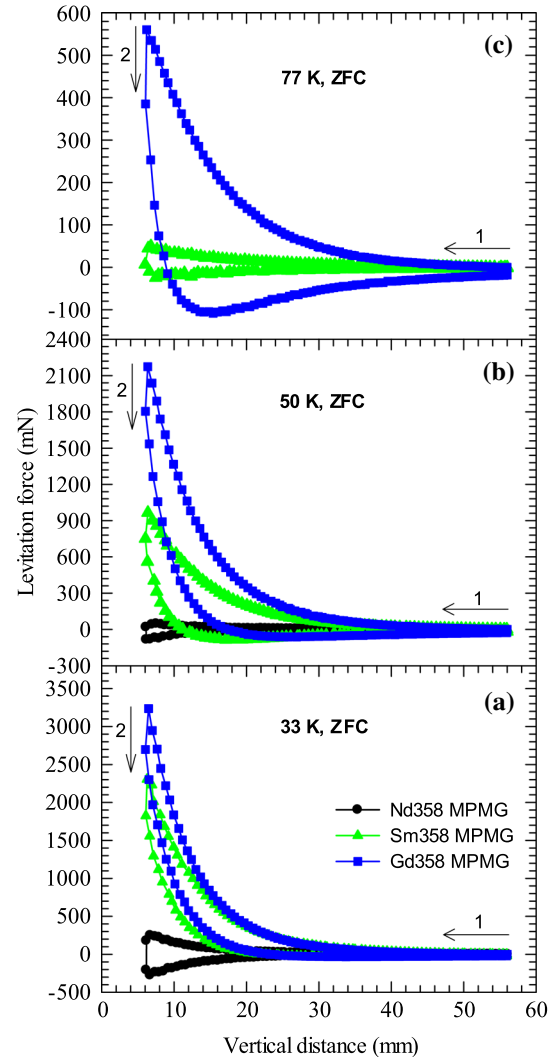


**Figure 10** Variations of levitation force versus vertical distance at a 33 K, b 50 K, and c 77 K. 1 and 2 symbolize moving toward HTSC and moving away from HTSC, in turn.

sample, and almost no weak-link taking into account the structural property results. Because in such a case, the value of  $r$  is large, and therefore  $F_{z,R}$  value ascends according to Eq. (6) [31]. Similarly, the highest  $F_{z,A}$  value belongs to Nd358 MPMG with -277 mN, whereas the lowest  $F_{z,A}$  value belongs to Sm358 MPMG with -29 mN. It is known that the greater



**Table 5** The maximum repulsive and attractive forces at different temperatures

| Sample     | 33 K           |          |                | 50 K           |          |                | 77 K           |          |                |
|------------|----------------|----------|----------------|----------------|----------|----------------|----------------|----------|----------------|
|            | $F_{z,R}$ (mN) | $\alpha$ | $F_{z,A}$ (mN) | $F_{z,R}$ (mN) | $\alpha$ | $F_{z,A}$ (mN) | $F_{z,R}$ (mN) | $\alpha$ | $F_{z,A}$ (mN) |
| Nd358 MPMG | 274            | 0.137    | – 277          | 51             | 0.124    | – 85           | –              | –        | –              |
| Sm358 MPMG | 2410           | 0.135    | – 29           | 1015           | 0.116    | – 85           | 48             | 0.082    | – 25           |
| Gd358 MPMG | 3449           | 0.157    | – 32           | 2301           | 0.133    | – 63           | 596            | 0.103    | – 109          |

the magnetic field entrapped by a superconducting sample is, the greater the  $F_{z,A}$  value is [29]. Based on this finding, it can be said that the magnetic field trapped by the Nd358 sample is greater. Moreover, in another study [12] it was stated that  $J_c$  improved by substituting Nd for Y for a RE358 SSR, and that the possible reason for this was lattice defects that enhance the flux pinning. Accordingly, it was believed that the  $F_{z,A}$  value of Nd358 MPMG sample was high since it had the defects such as weak-link, porosity, and impurity phases observed in the POM micrograph (Figure 5a) and also the defects such as oxygen deficiency that causes low orthorhombicity (Table 1) calculated from the XRD pattern.

The variation of the levitation force of the samples versus the vertical distance at 50 K is displayed in Figure 10b. Although the maximum  $F_{z,R}$  value belongs to the Gd358 MPMG sample with 2301 mN, the minimum  $F_{z,R}$  value belongs to the Nd358 MPMG sample with 51 mN (Table 5). Likewise, while the largest  $F_{z,A}$  value belongs to the samples of Nd358 and Sm358 MPMG with -85 mN, the smallest  $F_{z,A}$  value belongs to the Gd358 MPMG sample with -63 mN.

The variation of the levitation force of the samples with the vertical distance at 77 K is pictured in Figure 10c. Levitation force of the Nd358 MPMG sample was determined to be absent. This can be because the  $T_c^{\text{offset}}$  value (Figure 6a) obtained from the  $R$ - $T$  graph is less than 77 K. Apart from the sample Nd358 MPMG, the sample with a maximum  $F_{z,R}$  value of 596 mN is Gd358 MPMG, whereas the sample with a minimum  $F_{z,R}$  value of 48 mN is Sm358 MPMG (Table 5). The  $F_{z,R}$  of the Gd358 MPMG sample in this study is bigger than 170 mN measured for the Y358 MPMG sample in another study [14]. One reason for this is the presence of Gd211 particles detected in the POM micrograph as shown in the inset of Figure 5c [44]. Similarly, the sample with the highest  $F_{z,A}$  value

was Gd358 MPMG with -109 mN, while the sample with the lowest  $F_{z,A}$  value was -25 mN and Sm358 MPMG.

It was deduced that the maximum value of  $F_{z,R}$  increased gradually with 77 K, 50 K, and 33 K temperatures, and besides the sample with the best values was Gd358 MPMG. By virtue of the fact that the  $\alpha$  value given in Table 5 increased with reducing temperature, it was concluded that there was an exponentially proportional relationship between  $F_{z,R}$  and temperature. It is obvious that the  $J_c$  of a superconducting sample enhances exponentially as the temperature decreases [45]. Hence,  $F_{z,R}$  which is proportional to  $J_c$ , is expected to ascend with regard to Eq. (6).

It was comprehended that the relationship between the maximum value of  $F_{z,A}$  and 77 K, 50 K, 33 K temperatures differed in accordance with sample. With reducing temperature, the  $F_{z,A}$  value increases for Nd358 MPMG, decreases gradually for the Gd358 MPMG, and fluctuates for Sm358 MPMG. Usually,  $F_{z,A}$  is known to be caused by flux pinning, in other words, by trapping of the applied magnetic field [46–48]. Based on this, it can be stated that the effective mechanisms for flux pinning might be in different types in accordance with the sample or production technique and might also have a different attitude in terms of the measurement temperature. The attitude for Gd358 MPMG can be originated in both the increase of  $J_c$  and the decrease of Bean penetration depth  $\delta = H/J_c$  ( $H$ , the tangential component of the magnetic field on the HTSC surface) [49].

The detailed levitation analysis of the Gd358 MPMG, which stands out among the samples, is shown in Figure 11. As the temperature of the sample decreases, the  $F_{z,R}$  value enhances, and especially the enhancement between 77 and 50 K is higher (Figure 11a). This situation complies with the relationship

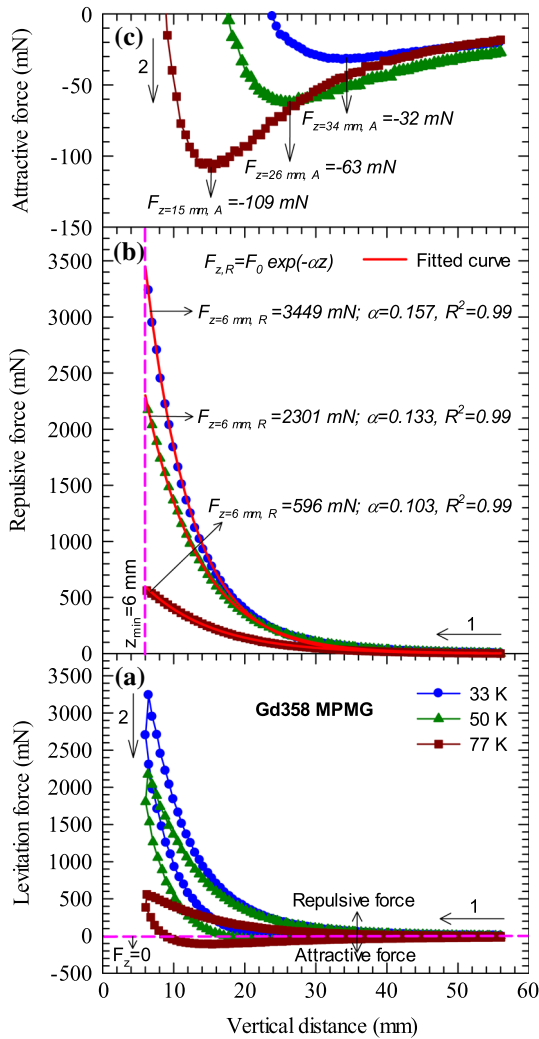


**Figure 11** Levitation analysis of Gd358 MPMG sample: **a** different temperatures, **b** repulsive force, and **c** attractive force.

$B_{c2}$ ,  $B_{c1} \propto 1 - (T/T_c)^2$  [50, 51] in the  $B$ - $T$  phase diagram. In addition, when taking into consideration the experimental data, the  $\alpha$  of the fitted curve with regard to Eq. (5) for 77 K, 50 K, and 33 K are, respectively, 0.103 ( $R^2 = 0.99$ , the coefficient of determination), 0.133 ( $R^2 = 0.99$ ) and 0.157 ( $R^2 = 0.99$ ) (Figure 11b). It was realized that there was a strong correlation between temperature and the  $\alpha$  value; that is, the lower the temperature was, the higher  $\alpha$  value was. Similarly, as the temperature of the sample drops, the value of  $F_{z,A}$  decreases and especially the decrease between 77 and 50 K is greater. This behavior is contrary to the behavior of  $F_{z,R}$ , and maybe elucidated as follows: An important feature for magnetic transportation systems of the sample prepared by melt technique such as MPMG is its

attractive or suspension-type force; such a force arises if  $B_z > B_{c1}$ ; it is a measure of trapped flux [52]. When  $B_{c1} \propto 1 - (T/T_c)^2$  is considered, the value of  $F_{z,A}$  became smaller since the trapped flux is less in case of  $T \rightarrow 0$  K under the ZFC regime. The maximum values of  $F_{z,A}$  are  $-109$  mN at  $z = 15$  mm for 77 K,  $-63$  mN at  $z = 26$  mm for 50 K, and  $-32$  mN at  $z = 34$  mm for 33 K (Figure 11c). It was determined that with the decrease of the temperature, the value of  $z$  corresponding to the maximum of  $F_{z,A}$  enlarged (i.e., not constant as in  $F_{z,R}$ ).

Overall evaluations showed that the Gd358 MPMG sample for the repulsive force and the Nd358 MPMG sample for the attractive force gave good results. It was believed that bulk Gd358 HTSC sample would be an innovative product considering the application at 77 K liquid nitrogen temperature especially in terms of cost.

### Conclusions

Bulk  $RE_3(Nd, Sm, Gd)Ba_5Cu_8O_y$  high-temperature superconductors were produced by the modified Melt-Powder-Melt-Growth technique. For future researchers of RE358 superconductors, the significant structural, electrical, and levitation results from the present study can be summarized as follows:

- The sample with high bulk density and hence low porosity was found to be Gd358 MPMG.
- The presence of minor phases such as RE211 was detected from the XRD results, although the major phase was the superconducting phase. It was confirmed that the number of minor phases was slightly higher in the Gd358 MPMG sample than the others.
- From the polarized optical microscope micrograph, it was observed that the sample with less weak-link, large superconducting grains, small RE211 particles and their homogeneous distribution, and low pore was generally the Gd358 MPMG sample. POM results are in good agreement with the bulk density and XRD results.
- It was determined that the best results of the  $T_c^{onset}$ ,  $T_c^{offset}$ , and  $\Delta T_c$  critical temperatures with/without applied magnetic field belonged to the Gd358 MPMG sample. POM results confirm this finding.

- When the irreversibility field and upper critical field were examined, it was concluded that the Gd358 MPMG sample had superior pinning ability in the inter-grain and intra-grain regions. That is,  $H_{irr}$  and  $H_{c2}$  values were improved with this sample.
- The minimum value of  $\beta$  from activation energy was calculated as 0.23 for the Gd358 MPMG sample. This value is quite good in comparison with the literature and indicates that the pinning energy is high.
- It was ascertained that the repulsive force increased gradually with measurement temperatures of 77 K, 50 K, and 33 K. After a detailed analysis, it was decided that there was a strong correlation between temperature and  $\alpha$  value estimated from the equation  $F_{z,R}$ . The maximum  $F_{z,R}$  value was obtained in the Gd358 MPMG sample at all temperatures. Results of structural and electrical properties verify these findings.
- The relationship between the maximum value of the attractive force and the temperatures of 77 K, 50 K, and 33 K was deduced to be different than the sample.
- The highest  $F_{z,A}$  value at 33 K was measured for the Nd358 MPMG sample. This most likely means that the magnetic field trapped by the Nd358 MPMG sample is greater. However, the  $F_{z,A}$  value at 77 K could not be measured for the Nd358 MPMG sample. This situation is consistent with the electrical property result.
- From an economic point of view, it is thought that the Gd358 HTSC sample would be an innovative product.

Further studies on the production of single-phase, the kinetics of phase formation, the contribution of secondary phases, the magnetic property, mechanical property, and levitation property such as field-cooled regime, loops, stiffness, relaxation of Gd358 superconducting material are strongly advised.

## Acknowledgements

This study was supported by a grant (contract no: 2010.111.001.1) from the Scientific Research Projects Coordination Unit of Karadeniz Technical University.

## References

- [1] Tair F, Carreras L, Camps J et al (2017) Melting temperature of  $YBa_2Cu_3O_{7-x}$  and  $GdBa_2Cu_3O_{7-x}$  at subatmospheric partial pressure. *J Alloys Compd* 692:787–792. <https://doi.org/10.1016/j.jallcom.2016.08.072>
- [2] Wang YN, Yang WM, Yang PT et al (2017) Influence of trapped field on the levitation force of SmBCO bulk superconductor. *Physica C* 542:28–33. <https://doi.org/10.1016/j.physc.2017.09.004>
- [3] Yokoyama K, Katsuki A, Miura A, Oka T (2018) Enhancement of trapped magnetic field using a large-size REBCO bulk in a desktop type superconducting bulk magnet. *IEEE Trans Appl Supercond* 28:1–4. <https://doi.org/10.1109/TASC.2017.2782680>
- [4] Osipov M, Abin D, Pokrovskii S, Rudnev I (2017) Levitation force of magnetized HTS tape stacks. *IEEE Trans Appl Supercond* 27:1–4. <https://doi.org/10.1109/TASC.2017.2668070>
- [5] Topal U, Akdogan M (2012) The role of oxygenation on superconducting properties of  $RE_3Ba_5Cu_8O_{18}$  (RE=Y, Sm and Nd) compounds. *J Supercond Nov Magn* 25:239–244. <https://doi.org/10.1007/s10948-011-1285-3>
- [6] Wu MK, Ashburn JR, Torng CJ et al (1987) Superconductivity at 93 K in a new mixed-phase Y-Ba-Cu-O compound system at ambient pressure. *Phys Rev Lett* 58:908. <https://doi.org/10.1103/PhysRevLett.58.908>
- [7] Marsh P, Fleming RM, Mandich ML et al (1988) Crystal structure of the 80 K superconductor  $YBa_2Cu_4O_8$ . *Nature* 334:141–143. <https://doi.org/10.1038/334141a0>
- [8] Bordet P, Chaillout C, Chenavas J et al (1988) Structure determination of the new high-temperature superconductor  $Y_2Ba_4Cu_7O_{14+x}$ . *Nature* 334:596–598. <https://doi.org/10.1038/334596a0>
- [9] Aliabadi A, Akhavan Farshchi Y, Akhavan M (2009) A new Y-based HTSC with  $T_c$  above 100 K. *Physica C* 469:2012–2014. <https://doi.org/10.1016/j.physc.2009.09.003>
- [10] Topal U, Akdogan M, Ozkan H (2011) Electrical and structural properties of  $RE_3Ba_5Cu_8O_{18}$  (RE=Y, Sm and Nd) superconductors. *J Supercond Nov Magn* 24:2099–2102. <https://doi.org/10.1007/s10948-011-1176-7>
- [11] Aliabadi A, Akhavan-Farshchi Y, Akhavan M (2014) Flux dynamics in Y358 and Gd358 superconductors. *J Supercond Nov Magn* 27:741–748. <https://doi.org/10.1007/s10948-013-2367-1>
- [12] Rekaby M, Roumié M, Abou-Aly A et al (2014) Magnetoresistance study of  $Y_3Ba_5Cu_8O_{18}$  superconducting phase substituted by  $Nd^{3+}$  and  $Ca^{2+}$  ions. *J Supercond Nov Magn* 27:2385–2395. <https://doi.org/10.1007/s10948-014-2572-6>

- [13] Kutuk S, Bolat S, Terzioglu C, Altintas SP (2015) An investigation of magnetoresistivity properties of an Y3Ba5Cu8Oy bulk superconductor. *J Alloys Compd* 650:159–164. <https://doi.org/10.1016/j.jallcom.2015.06.273>
- [14] Bolat S, Kutuk S (2012) Fabrication of the new Y3Ba5Cu8Oy superconductor using melt–powder–melt–growth method and comparison with YBa2Cu3O7–x. *J Supercond Nov Magn* 25:731–738. <https://doi.org/10.1007/s10948-011-1332-0>
- [15] Kutuk S, Bolat S, Başoğlu M, Öztürk K (2009) Comparison of levitation force relative to thickness of disk shaped YBa2Cu3O7-x prepared by MPMG and FQMG processes. *J Alloys Compd* 488:425–429. <https://doi.org/10.1016/j.jallcom.2009.08.149>
- [16] Kutuk S, Bolat S (2018) Levitation force of (RE)BCO-358 bulk superconductors. *AIP Conf Proc* 2042:020033. <https://doi.org/10.1063/1.5078905>
- [17] Muralidhar M, Chauhan HS, Saitoh T et al (1997) Effect of mixing three rare-earth elements on the superconducting properties of REBa2Cu3Oy. *Supercond Sci Technol* 10:663–670. <https://doi.org/10.1088/0953-2048/10/9/006>
- [18] Murakami M, Oyama T, Fujimoto H et al (1991) Melt processing of bulk high Tc superconductors and their application. *IEEE Trans Magn* 27:1479–1486. <https://doi.org/10.1109/20.133464>
- [19] Matsui M, Murakami M (2003) Enhancement of the trapped-fields and mechanical properties of Nd–Ba–Cu–O bulk superconductors. *Ceram Int* 29:117–137. [https://doi.org/10.1016/S0272-8842\(02\)00094-9](https://doi.org/10.1016/S0272-8842(02)00094-9)
- [20] Hamadneh I, Yaseen N, Abdallat Y et al (2016) The sintering effect on the phase formation and transport current properties of SmBa2Cu3O7– $\delta$  ceramic prepared from nano-coprecipitated precursors. *J Supercond Nov Magn* 29:829–834. <https://doi.org/10.1007/s10948-015-3341-x>
- [21] Campá JA, de Salazar JMG, Gutiérrez-Puebla E et al (1988) Crystal structure of the oxides BaCuGd2O5 and Ba2Cu3GdO7-x. *Phys Rev B* 37:529–532. <https://doi.org/10.1103/PhysRevB.37.529>
- [22] Slimani Y, Hannachi E, Hamrita A et al (2015) Energy dissipation mechanisms in polycrystalline superconductor Y3Ba5Cu8Oy. *J Supercond Nov Magn* 28:487–492. <https://doi.org/10.1007/s10948-014-2745-3>
- [23] Vanderah TA (1992) *Chemistry of superconductor materials*. Noyes Publications, New Jersey
- [24] Kütük S, Bolat S, Öztürk K et al (2011) Microstructure study at different thicknesses of disc-shaped YBa2Cu3O7–x prepared by FQMG method. *J Supercond Nov Magn* 24:471–474. <https://doi.org/10.1007/s10948-010-0974-7>
- [25] Ghahramani S, Shams G, Soltani Z (2021) Comparative investigation of the effect of titanium oxide nanoparticles on some superconducting parameters of Y3Ba5Cu8O18 $\pm\delta$  and Y1Ba2Cu3O7– $\delta$  composites. *J Electron Mater* 50:4727–4740. <https://doi.org/10.1007/S11664-021-09012-5>
- [26] Shoushtari MZ, Heidarzadeh G, Ghahfarokhi SEM (2018) An Investigation of Y3Ba5Cu8O18 doping with Ag nanoparticles and Its application as superconductor. *J Supercond Nov Magn* 31:3475–3483. <https://doi.org/10.1007/s10948-018-4581-3>
- [27] Benzi P, Bottizzo E, Rizzi N (2004) Oxygen determination from cell dimensions in YBCO superconductors. *J Cryst Growth* 269:625–629. <https://doi.org/10.1016/j.jcrysgro.2004.05.082>
- [28] Krüger C, Conder K, Schwer H, Kaldis E (1997) The dependence of the lattice parameters on oxygen content in orthorhombic YBa2Cu3O6+x: a high precision reinvestigation of near equilibrium samples. *J Solid State Chem* 134:356–361. <https://doi.org/10.1006/jssc.1997.7579>
- [29] Murakami M (1992) Processing of bulk YBaCuO. *Supercond Sci Technol* 5:185–203. <https://doi.org/10.1088/0953-2048/5/4/001>
- [30] Diko P (2006) Microstructural limits of TSMG REBCO bulk superconductors. *Physica C* 445:323–329. <https://doi.org/10.1016/j.physc.2006.06.030>
- [31] Kütük S, Bolat S, Öztürk K et al (2011) Levitation force density on different thicknesses of YBa2Cu3O7-x bulk superconductor fabricated by FQMG process. *J Supercond Nov Magn* 24:475–479. <https://doi.org/10.1007/s10948-010-0975-6>
- [32] Zhou JP, Dou SX, Liu HK et al (1989) Crystallite alignment of YBa2Cu3O7–x through texture growth. *Supercond Sci Technol* 2:212–215. <https://doi.org/10.1088/0953-2048/2/4/002>
- [33] Yoo SI, Sakai N, Takaichi H et al (1994) Melt processing for obtaining NdBa2Cu3Oy superconductors with high Tc and large Jc. *Appl Phys Lett* 65:633–635. <https://doi.org/10.1063/1.112254>
- [34] Gupta A, Deshpande AJ, Awana VPS et al (2007) Flux line motion in superconducting (YBa2Cu3O7–d)1–x/(SiO2)x composite systems in high magnetic fields. *Supercond Sci Technol* 20:1084–1091. <https://doi.org/10.1088/0953-2048/20/10/031>
- [35] Gamchi HS, Russell GJ, Taylor KNR (1994) Resistive transition for YBa2Cu3O7– $\delta$ -Y2BaCuO5 composites: influence of a magnetic field. *Phys Rev B* 50:12950–12958. <https://doi.org/10.1103/PhysRevB.50.12950>
- [36] Oh B, Char K, Kent AD et al (1988) Upper critical field, fluctuation conductivity, and dimensionality of YBa2Cu3O7-x. *Phys Rev B* 37:7861–7864. <https://doi.org/10.1103/PhysRevB.37.7861>



- [37] Kim JH, Dou SX, Shi DQ et al (2007) Study of MgO formation and structural defects in in situ processed MgB<sub>2</sub>/Fe wires. *Supercond Sci Technol* 20:1026–1031. <https://doi.org/10.1088/0953-2048/20/10/023>
- [38] Dogruer M, Terzioglu C, Gorur O, Yildirim G (2014) Importance of magnetoresistivity properties and decrement of the flux pinning energy in YBa<sub>2</sub>Cu<sub>3</sub>O<sub>7-x</sub> bulk superconductors doped with Gd nanoparticles. *J Supercond Nov Magn* 27:681–686. <https://doi.org/10.1007/s10948-013-2353-7>
- [39] Yang P-T, Yang W-M, Abula Y et al (2017) Effect of Li doping on the superconducting properties of single domain GdBCO bulks fabricated by the top-seeded infiltration and growth process. *Ceram Int* 43:3010–3014. <https://doi.org/10.1016/j.ceramint.2016.11.094>
- [40] Palstra TTM, Batlogg B, Van Dover RB et al (1990) Dissipative flux motion in high-temperature superconductors. *Phys Rev B*. <https://doi.org/10.1103/PhysRevB.41.6621>
- [41] Dogruer M, Zalaoglu Y, Varilci A et al (2012) A study on magnetoresistivity, activation energy, irreversibility and upper critical field of slightly Mn Added Bi-2223 superconductor ceramics. *J Supercond Nov Magn* 25:961–968. <https://doi.org/10.1007/s10948-012-1403-x>
- [42] Yang WM, Zhou L, Feng Y et al (1998) The grain-alignment and its effect on the levitation force of melt processed YBCO single-domained bulk superconductors. *Physica C* 307:271–276. [https://doi.org/10.1016/S0921-4534\(98\)00414-6](https://doi.org/10.1016/S0921-4534(98)00414-6)
- [43] Hull JR, Passmore JL, Mulcahy TM, Rossing TD (1994) Stable levitation of steel rotors using permanent magnets and high-temperature superconductors. *J Appl Phys* 76:577–580. <https://doi.org/10.1063/1.357115>
- [44] Yang W, Yuan X, Zhang C (2019) How to control the Gd<sub>2</sub>11 particles and enhance the levitation force of single domain GdBCO bulks prepared by the Gd+011 TSIG method. *IEEE Trans Appl Supercond* 29:1–5. <https://doi.org/10.1109/TASC.2019.2909835>
- [45] Crabtree GW, Liu JZ, Umezawa A et al (1987) Large anisotropic critical magnetization currents in single-crystal YBa<sub>2</sub>Cu<sub>3</sub>O<sub>7-x</sub>. *Phys Rev B* 36:4021–4024. <https://doi.org/10.1103/PhysRevB.36.4021>
- [46] Brandt EH (1988) Friction in levitated superconductors. *Appl Phys Lett* 53:1554–1556. <https://doi.org/10.1063/1.100435>
- [47] Unsworth J, Du J, Crosby BJ, Macfarlane JC (1993) Magnetic levitation force measurement on high T<sub>c</sub> superconducting ceramic/polymer composites. *IEEE Trans Magn* 29:108–112. <https://doi.org/10.1109/20.195554>
- [48] Yoo SI, Fujimoto H, Sakai N, Murakami M (1997) Melt-processed LRE-Ba-Cu-O superconductors and prospects for their applications. *J Alloys Compd* 250:439–448. [https://doi.org/10.1016/S0925-8388\(96\)02864-2](https://doi.org/10.1016/S0925-8388(96)02864-2)
- [49] Zeisberger M, Gawalek W, Giunchi G (2005) Magnetic levitation using magnesium diboride. *J Appl Phys* 98:023905. <https://doi.org/10.1063/1.1985972>
- [50] Parinov IA (2007) *Microstructure and properties of high-temperature superconductors*. Springer, Berlin
- [51] Hook JR, Hall HE (1999) *Solid state physics*. Wiley, England
- [52] Moon FC (1995) *Superconducting levitation*. Wiley, Germany

**Publisher's Note** Springer Nature remains neutral with regard to jurisdictional claims in published maps and institutional affiliations.